NeuroImage 310 (2025) 121132

Contents lists available at ScienceDirect

NeuroImage

journal homepage: www.elsevier.com/locate/ynimg

White matter microstructure links with brain, bodily and genetic attributes in adolescence, mid- and late life

Max Korbmacher [a,b,c,*], Mario Tranfa [d,e], Giuseppe Pontillo [d,e,f], Dennis van der Meer [g], Meng-Yun Wang [h], Ole A. Andreassen [g], Lars T. Westlye [i,j], Ivan I. Maximov [c]

[a] Neuro-SysMed Center of Excellence for Clinical Research in Neurological Diseases, Department of Neurology, Haukeland University Hospital, Bergen, Norway
[b] Mohn Medical Imaging and Visualization Centre (MMIV),Department of Radiology, Haukeland University Hospital, Bergen, Norway
[c] Department of Health and Functioning, Western Norway University of Applied Sciences, Bergen, Norway
[d] Department of Advanced Biomedical Sciences, University "Federico II", Naples, Italy
[e] Department of Radiology and Nuclear Medicine, Vrije Universiteit Amsterdam,Amsterdam UMC location VUMC, Amsterdam, The Netherlands
[f] Department of Brain Repair & Rehabilitation, UCL Queen Square Institute of Neurology,University College London, London, United Kingdom
[g] Center for Precision Psychiatry, University of Oslo and Oslo University Hospital, Oslo, Norway
[h] Max Planck Institute for Psycholinguistics, Nijmegen, Netherlands
[i] Department of Psychology, University of Oslo, Oslo, Norway
[j] KG Jebsen Centre for Neurodevelopmental Disorders, University of Oslo, Oslo, Norway

ARTICLE INFO

Dataset link: https://www.ukbiobank.ac.uk, https://abcdstudy.org, https://github.com/MaxKorbmacher/dMRI_approach_comparison

Keywords:
White matter microstructure
Diffusion MRI
Magnetic resonance imaging
Brain ageing

ABSTRACT

Advanced diffusion magnetic resonance imaging (dMRI) allows one to probe and assess brain white matter (WM) organisation and microstructure in vivo. Various dMRI models with different theoretical and practical assumptions have been developed, representing partly overlapping characteristics of the underlying brain biology with potentially complementary value in the cognitive and clinical neurosciences. To which degree the different dMRI metrics relate to clinically relevant geno- and phenotypes is still debated. Hence, we investigate how tract-based and whole WM skeleton parameters from different dMRI approaches associate with clinically relevant and white matter-related phenotypes (sex, age, pulse pressure (PP), body-mass-index (BMI), brain asymmetry) and genetic markers in the UK Biobank (UKB, n=52,140) and the Adolescent Brain Cognitive Development (ABCD) Study (n=5,844). In general, none of the imaging approaches could explain all examined phenotypes, though the approaches were overall similar in explaining variability of the examined phenotypes. Nevertheless, particular diffusion parameters of the used dMRI approaches stood out in explaining some important phenotypes known to correlate with general human health outcomes. A multi-compartment Bayesian dMRI approach provided the strongest WM associations with age, and together with diffusion tensor imaging, the largest accuracy for sex-classifications. We find a similar pattern of metric and tract-dependent asymmetries across datasets, with stronger asymmetries in ABCD data. The magnitude of WM associations with polygenic scores as well as PP depended more on the sample, and likely age, than dMRI metrics. However, kurtosis was most indicative of BMI and potentially of bipolar disorder polygenic scores. We conclude that WM microstructure is differentially associated with clinically relevant pheno- and genotypes at different points in life.

1. Introduction

White matter (WM) is characterised by bundles of axonal neurites that stretch across the human brain. By connecting grey matter neurons with each other, fibre bundles allow for neural communication across the brain. Diffusion magnetic resonance imaging (dMRI) probes *in vivo* brain organisation and microstructure, and is a particularly powerful tool for WM mapping. DMRI allows for quantification and visualisation of different brain tissue features. Recent advances (Novikov et al., 2019, 2018b; Reisert et al., 2017; Kaden et al., 2016a,b; Fieremans et al., 2011) have led to many proposed approaches to model and characterise WM beyond commonly used diffusion tensor imaging (DTI) (Novikov et al., 2018a) and approaches exploiting non-Gaussian diffusivity (kurtosis) (Jensen et al., 2005; Fieremans et al., 2011). However, such approaches are limited by not being able to address the complexity of the tissue structure, for instance, crossing fibres or microscopic cellular features (Dell'Acqua and Tournier, 2019; Novikov

* Correspondence to: Neuro-SysMed group, Department of Neurology, Haukeland University Hospital, Haukelandsveien 22, 5009 Bergen, Norway.
E-mail address: max.korbmacher@uib.no (M. Korbmacher).

https://doi.org/10.1016/j.neuroimage.2025.121132
Received 27 November 2024; Received in revised form 2 March 2025; Accepted 7 March 2025
Available online 15 March 2025

et al., 2019). Hence, new approaches were developed to more adequately assess WM microstructure. These approaches generally rely on the standard model of diffusion, which separates intra- and extra-axonal space (Novikov et al., 2019, 2018b; Reisert et al., 2017), with different assumptions about the characteristics of these intra- and extra-axonal compartments (e.g., modelling diffusion within impermeable cylinders or spheres of different sizes). Based on such assumptions, one can derive a range of scalar parameters reflecting different WM features within the framework of the standard diffusion model or empiric diffusion representation. As a result, there is a multitude of diffusion parameters often having closely related meaning or presenting strong correlations between approaches (Korbmacher et al., 2023a; Beck et al., 2021). For each parameter, one can create voxel-wise maps or average across WM tracts and regions. Thus, these scalar maps offer quantitative features of WM organisation and structure.

As the parameters across dMRI approaches describe diffusion, they are also related to each other. However, their sensitivity to and complementary value for predicting clinically relevant traits is unclear. Mapping such relationships can inform future selections of dMRI approaches to extract meaningful metrics to answer specific research questions about the role of WM in health and disease.

Hence, in the present comparative analyses, we present effect sizes (associations and group differences) for a range of clinically relevant metrics and the parameters of six dMRI approaches in two large-scale MRI datasets, the UK Biobank (UKB) and the Adolescent Brain Cognitive Development (ABCD) Study. The non-WM metrics were chosen based on previous evidence indicating WM-associations, and their general clinical relevance for cardiometabolic, neurological and psychiatric disorders. These metrics include sex, age, brain asymmetry, body-mass-index, pulse pressure, and polygenic risk scores. We highlight the strongest effects to assess dMRI approaches as a whole (such as Diffusion Tensor Imaging), spatial specificity on the tract-level (such as the cingulum-hippocampus tract), and metric-specificity (e.g., the intra-axonal water fraction from the Bayesian multi-compartment approach).

2. Methods

2.1. Samples

We analysed diffusion data from two big MRI studies: UK Biobank (Miller et al., 2016) and ABCD (Casey et al., 2018). We obtained $N_{total} = 52{,}140$ datasets, with $N_{ABCD} = 5{,}844$ and $N_{UKB} = 46{,}196$.

Due to variability in ethnicity, relevant to polygenic assessments, we controlled for participants' ethnicity in all genotype-related analyses. Brain volume was used as a covariate in all analyses to account for difference in brain size.

2.2. MRI acquisition and post-processing

UKB MRI data acquisition procedures and protocols are described elsewhere (Alfaro-Almagro et al., 2018; Miller et al., 2016; Sudlow et al., 2015), see https://www.fmrib.ox.ac.uk/ukbiobank/protocol/. For ABCD acquisition protocols see https://abcdstudy.org/scientists/protocols/. The dMRI protocols in these studies are different and optimised for different diffusion approaches.

After access to the raw dMRI data, we processed the data using an optimised pipeline (Maximov et al., 2019), including corrections for noise (Veraart et al., 2016), Gibbs ringing (Kellner et al., 2016), susceptibility-induced and motion distortions, and eddy current artifacts (Andersson and Sotiropoulos, 2016). Isotropic 1 mm^3 Gaussian smoothing for UKB and 0.8 mm^3 in ABCD was carried out using FSL's (Smith et al., 2004; Jenkinson et al., 2012) *fslmaths* (FSL version 6.0.1). Employing the multi-shell data, DTI, DKI (Jensen et al., 2005) and WMTI (Fieremans et al., 2011) parameters were estimated using Matlab 2017b code (https://gitgub.com/NYU-DiffusionMRI/DESIGNER). SMT (Kaden et al., 2016b), mcSMT (Kaden et al., 2016a) parameters were estimated using original (Kaden et al., 2016a,b) in-house C++ code (https://github.com/ekaden/smt). BRIA estimates were evaluated with the original (Reisert et al., 2017) Matlab code (https://bitbucket.org/reisert/baydiff/src/master/).

We used Tract-based Spatial Statistics (TBSS) (Smith et al., 2006), as part of FSL (Smith et al., 2004; Jenkinson et al., 2012). Initially, all brain-extracted (Smith, 2002) fractional anisotropy (FA) images were aligned to MNI space using non-linear transformation (FNIRT) (Jenkinson et al., 2012). Next, the mean FA image and mean FA skeleton were derived. Each diffusion scalar map was projected onto the mean FA skeleton using TBSS. To provide a quantitative description of diffusion parameters at the tract level, we used the John Hopkins University (JHU) atlas (Mori et al., 2006; Hua et al., 2008) 20 tract averages based on a probabilistic WM atlas for each of the 26 parameters, totalling 520 values per individual. We additionally computed the skeleton average for each of the 26 parameters.

We processed 26 diffusion parameters (see for overview Appendix M) from the following diffusion approaches: the Bayesian Rotationally Invariant Approach (BRIA) (Reisert et al., 2017), Diffusion Kurtosis Imaging (DKI) (Jensen et al., 2005), Diffusion Tensor Imaging (DTI) (Basser et al., 1994), the Spherical Mean Technique (SMT) (Kaden et al., 2016b), and its multicompartment extension (SMTmc) (Kaden et al., 2016a), and White Matter Tract Integrity (WMTI) (Fieremans et al., 2011).

Quality control comprised of the YTTRIUM method (Maximov et al., 2021) which converts global dMRI scalar metrics into 2D format using a structural similarity extension of each scalar map to their mean image in order to create a 2D distribution of image and diffusion parameters. Non-clusterised values are then excluded. Additional exclusions entailed tract-based values exceeding 5 standard deviations from the mean in each parameter. This procedure led to 697 exclusions in ABCD (11.93%) and 2,555 in the UKB data (5.53%). After merging the different diffusion scalars, we obtained a final sample of $N_{total} = 42{,}230$, with $N_{ABCD} = 5{,}147$ and $N_{UKB} = 37{,}083$, with UKB data representing 87.81% of the total sample. This includes the matched brain volume estimates from T_1-weighted data. For the cortical reconstruction of T_1-weighted data to obtain these volumes, we used Freesurfer legacy version 5.3.0. Here, we only considered the total cortical volume to be used as a covariate. Finally, we used COMBAT (Johnson et al., 2007) for harmonisation across scanner sites, while keeping variance in tact for sex and age. Note, however, that first, COMBAT does not remove all of the present variance with hence potentially scanner- or site-specific variance remaining. Second, due to potential group imbalances, COMBAT (or other similar methods) can lead to exaggerated effect estimates (Nygaard et al., 2016). To address both concerns, we included scanner as an additional covariate in our analyses.

2.3. Polygenic risk scores (PGRS)

We estimated PGRS for each participant with available genomic data, using LDPred2 (Privé et al., 2020) with default settings. As input for the PGRS, we used summary statistics from recent genome-wide association studies of Autism Spectrum Disorder (ASD) (Autism Spectrum Disorders Working Group of The Psychiatric Genomics Consortium, 2017), Major Depressive Disorder (MDD) (Wray et al., 2018), Schizophrenia (SCZ) (Trubetskoy et al., 2022), Attention Deficit Hyperactivity Disorder (ADHD) (Demontis et al., 2019), Bipolar Disorder (BIP) (Mullins et al., 2021), Obsessive Compulsive Disorder (OCD) (Arnold et al., 2018), Anxiety Disorder (ANX) (Otowa et al., 2016), and Alzheimer's Disease (AD) (Wightman et al., 2021). We used a minor allele frequency of 0.05, as the threshold most commonly used in PGRS studies of psychiatric disorders.

2.4. Cardiometabolic risk factors

We used a selection of cardiometabolic factors, which have previously been linked to WM (Korbmacher et al., 2024b, 2023b; Beck et al., 2022), and which were available in both datasets. Body-mass-index (BMI) was calculated as $weight(\mathrm{kg})/(height(\mathrm{m}))^2$ and PP (mmHg) as the difference between systolic and diastolic PP. For a better estimation of PP, we used the average of PPs derived from each automated reading.

2.5. Statistical analyses

For internal validation, we split the sample into a 80% discovery set ($N_{total} = 33{,}783$, with $N_{ABCD} = 4,117$ and $N_{UKB} = 29{,}666$) and a 20% replication set while weighting for the imbalanced dataset sizes (UKB: 87.81%). The replication set served to validate our findings.

First, we correlated all skeleton and tract-level average metrics with each other for a descriptive overview of associations between metrics across dMRI approaches.

Second, we used the WM parameters from each dMRI approach to classify participants' into males or females based on their tract-level metrics (M_1 to M_i) using logistic regression. Due to multicollinearity among the predictors, we used principal components analyses to obtain orthogonal predictors. As the 5 first components (PC_1 to PC_5) of the tract-level scalars of each dMRI approach explained between 60% and 90% of the variance, we limited the analysis to 5 PCs for these classifications and further analyses. This was leading to 7 classifications per dataset and additionally 7 classifications for the combined data (14 classifications in total).

$$\hat{Sex} = \left(1 + e^{-(\beta_0+\beta_1\times age+\beta_2\times scanner+\beta_3\times volume+\beta_4\times PC_1+\beta_5\times PC_2+\beta_6\times PC_3+\beta_7\times PC_4+\beta_8\times PC_5)}\right)^{-1} \quad (1)$$

To add explainability to the principal components (PC; used across analyses), we correlated each of the resulting five components (PC_j) with each tract-level metric (M_i) individually while controlling for covariates (scanner, sex, age) using simple linear regression models ($N_{tests} = 5(PCs) \times 26(metrics) = 130$). This approach was chosen in order to being able to correct for covariates:

$$\hat{PC}_j = \beta_0 + \beta_1 \times age + \beta_2 \times scanner + \beta_3 \times sex + \beta_4 \times volume + \beta_5 \times M_i \quad (2)$$

Third, we associated the aforementioned principal components (PC_j) and age, as well as skeleton-averaged metrics (S_l, $N_{associations} = 7(PC)+26(S) = 33$):

$$\hat{PC}_j \vee \hat{S}_l = \beta_0 + \beta_1 \times age + \beta_2 \times scanner + \beta_3 \times volume + \beta_4 \times sex \quad (3)$$

Fourth, we assessed tract asymmetries using paired-sample t-tests on each metric for each pair of *lateralised* tracts ($N_{t-tests} = 9(tracts) \times 26(metrics) = 234$).

Fifth, we assessed associations between the cardiovascular risk factors BMI and PP (PP) and the mentioned principal components (PC_j) and skeleton averages (S_l, $N_{associations} = 2(BMI \vee PP)\times(6(PC)+26(S)) = 64$):

$$\hat{BMI} \vee \hat{PP} = \beta_0 + \beta_1 \times PC_j \vee S_l + \beta_2 \times scanner + \beta_3 \times sex + \beta_4 \times volume + \beta_5 \times age \quad (4)$$

Sixth, we assessed associations between PGRS and principal components (PC) and skeleton averages (S). For that, we initially estimated the first principal component of the PGRS for common psychiatric disorders. For the associations between the PGRS for Alzheimer's disease, we used the raw value ($N_{associations} = 7\ (PGRS)\times\ 32$ (6 tract level models + 26 skeleton averages) = 224). To avoid confounding genetic effects of ethnicity, we also included ethnicity as a factor:

$$\hat{PGRS} = \beta_0 + \beta_1 \times PC_j \vee S_l + \beta_2 \times scanner + \beta_3 \times sex + \beta_4 \times age + \beta_5 \times ethnicity + \beta_6 \times volume \quad (5)$$

All analyses were executed on (a) the UKB data, (b) the ABCD data. There was only one exception where both datasets were analysed together: the correlations between the diffusion parameters, to showcase that the associations were robust, independent of the data composition. The data were scaled by subtracting the mean and dividing by the standard deviation, and standardised β coefficients were reported.

A total number of 699 analyses per dataset were conducted. We adjusted our α-level accordingly, using a conservative Bonferroni correction to control false positives, leading to $\alpha = 0.05/699 = 0.000071$.

Considering the tests with lowest power defined by 4 numerator degrees of freedom (see formulas above) and 3691 denominator degrees of freedom (based on the smallest sample, the training portion of the ABCD data, testing for BMI and PP), at an adjusted significance level of 0.0071% and 95% power, one can detect effects as low as Cohen's $f^2 = 0.011$, which closely translates to a coefficient of determination of $R^2 = 0.011$ or a correlation coefficient of $r = 0.104$, and a Cohen's $d = 0.209$. Using the same parameters on the minimum 29,648 denominator degrees of freedom in the UK Biobank, reflecting the analyses on the training UKB sample with the largest number of missingness, yielded minimum detectable effect sizes of $f^2 \approx R^2 = 0.001$, a correlation coefficient of $r = 0.0368$, and Cohen's $d = 0.074$. To establish comparability, we report standardised coefficients. All analyses were conducted in R, version 4.2.1.

3. Results

Skeleton-averaged metrics correlated conditionally in two clusters, describing (a) radial and axial diffusivity (b) FA and kurtosis. Notably, dependencies of water fraction metrics from the different diffusion approaches varied in their relationships with other metrics dependent on different diffusion protocols. Hence, partial voluming cannot be excluded in the presence of the free water compartment (Fig. 1).

Due to multicollinearity, we used the first five principal components of the respective dMRI approaches' tract-level estimates, instead of raw tract scores. Permutation-based statistical tests on the extracted components, or short: PCAtest (Camargo, 2022), indicated that there was significantly more correlational structure among the observed variables than expected by random chance, and that each of the five components were statistically significant ($p < 0.05$) across the examined diffusion approaches in each of the examined datasets with the exception of the spherical mean technique as well as white matter tract integrity in ABCD data, with only 3 significant components. The first two principal components generally explained together nearly 70% of the variance, with the exception of WMTI in the ABCD data, where the first two components explained 62.5% of the variance of the individual tract-level scalars. Scree plots showing the variance explained for each of the approaches and their combination can be found in Appendices A–B.

3.1. Sex classifications

The accuracy for sex classifications from principal components of tract-level scalars was similar across approaches and highly replicable, yet with DTI and BRIA performing slightly better in the UKB, and WMTI and DTI in the ABCD set (Table 1). Note, however, that Z-scores for the predictors were on average higher for cortical volume ($\bar{Z}_{UKB} = 71.78$, $\bar{Z}_{ABCD} = 23.42$) compared to the 5 principal components ($\bar{Z}_{UKB-PC1} = 8.74$, $\bar{Z}_{UKB-PC2} = 11.32$, $\bar{Z}_{UKB-PC3} = 13.49$, $\bar{Z}_{UKB-PC4} = 29.15$, $\bar{Z}_{UKB-PC5} = 18.11$; $\bar{Z}_{ABCD-PC1} = 6.94$, $\bar{Z}_{ABCD-PC2} = 4.09$, $\bar{Z}_{ABCD-PC3} = 4.52$, $\bar{Z}_{ABCD-PC4} = 6.54$, $\bar{Z}_{ABCD-PC5} = 7.06$). Nevertheless, the principal components' contributions were highly replicable and, for most components, every step increase in the rotated data (with all SDs > 3) significantly influenced the likelihood estimates for group memberships (Fig. 2).

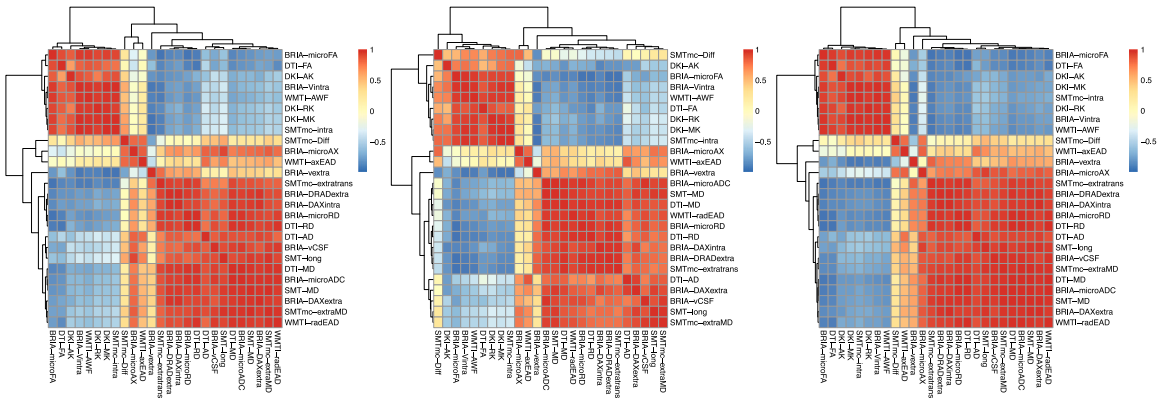

Fig. 1. Correlations between skeleton-level averaged metrics from each of the diffusion approaches. Panels from left to right indicate UKB, ABCD, and merged data (UKB and ABCD data). Correlations were clustered both column- and row-wise. BRIA = Bayesian Rotationally Invariant Approach. DKI = Diffusion Kurtosis Imaging. DTI = Diffusion Tensor Imaging. SMT = Spherical Mean Technique. SMTmc = SMT's multi-compartment version. WMTI = WM Tract Integrity. Metrics for each of the approaches are specified in Appendix M.

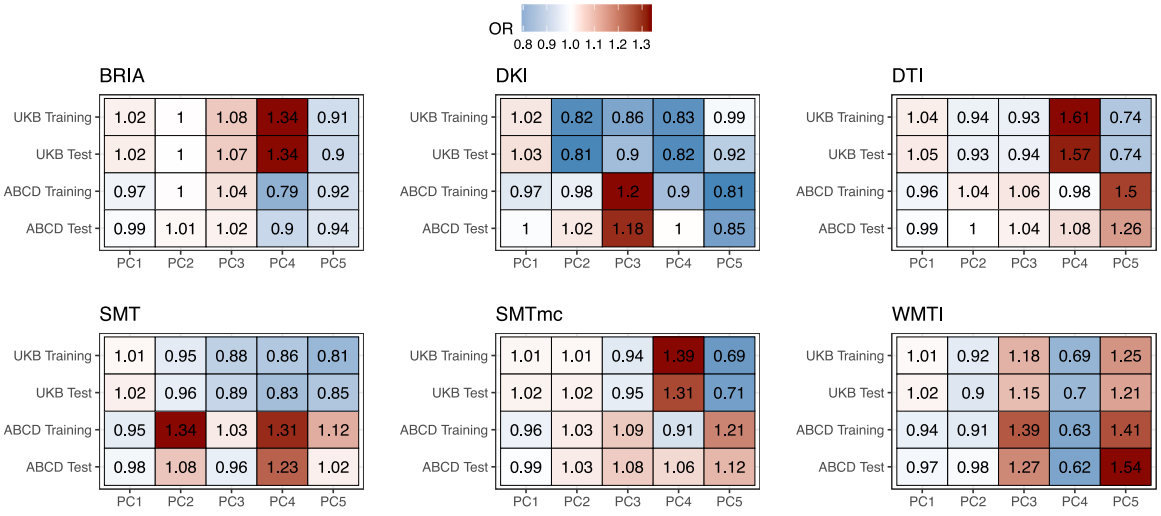

Fig. 2. Odds ratios (OR) indicating the contribution of the principal components to the sex-classifications. BRIA = Bayesin Rotationally Invariant Approach. DKI = Diffusion Kurtosis Imaging. DTI = Diffusion Tensor Imaging. SMT = Spherical Mean Technique. SMTmc = SMT's multi-compartment version. WMTI = White Matter Tract Integrity. Metrics for each of the approaches are specified in Appendix M. Only age associations for BRIA vCSF in the ABCD data set were not sufficiently powered ($r < 0.09$) and all other associations were significant ($p < 0.001$).

Table 1
Accuracy of sex-classification models in UKB and ABCD training and test datasets. Note that the individual level coordinates in the test data were predicted based on the training components' eigenvectors (scaling and centering based on the respective training sets).

Model	UKB train	UKB test	ABCD train	ABCD test	
1	BRIA	**75.48**	**75.33**	72.24	71.01
2	DKI	74.26	74.21	71.12	71.69
3	DTI	**76.08**	**76.37**	**72.77**	**72.28**
4	SMT	73.30	72.78	72.75	71.30
5	SMTmc	75.34	75.00	71.92	71.11
6	WMTI	74.84	74.52	**73.89**	**73.54**

When examining the corrected loadings of PCs with the strongest contributions to sex classifications (see Appendices C–L for overview of all corrected loading), the cingulum-hippocampus tract as well as uncinate fasciculus loaded strongest and most replicable on the corresponding components across datasets (Supplement N). While these correlations were tract-specific, they were not metric-specific.

Overall, sex differences were highly replicable: 93.26% of the effects observed in the UK Biobank and 80.38% of the effects in the ABCD study were of the same direction when comparing training and test data. Moreover, 76.35% of all effects replicated in both datasets.

These effects where on average small, after correcting for sex, age, scanner and brain volume across datasets when considering all effects $\bar{\beta} < 0.006$, or the tracts that loaded strongest on the respective PCs across features: hippocampal cingulum tract $\bar{\beta} < 0.008$, or uncinate fasciculus $\bar{\beta} < 0.004$.

3.2. Age associations

The variability in white matter microstructure metrics was more predictive of older than younger age, as suggested by stronger associations between model predicted age and chronological age in UKB ($r > 0.54$) compared to ABCD ($r > 0.21$; Table 2, for root mean square error estimates for the predictions see Supplementary Table P). Accordingly, white matter metric-derived components were predictive of age in UKB, but not ABCD data (Supplement O), suggesting potential effects of the limited age-span in the ABCD sample.

To also assess tract-level associations with age, we assessed the strongest replicable correlates of the principle components from UKB data (see Supplement O) in both UKB and ABCD, which were the same set components for BRIA, DTI, SMTmc and WMTI as for the

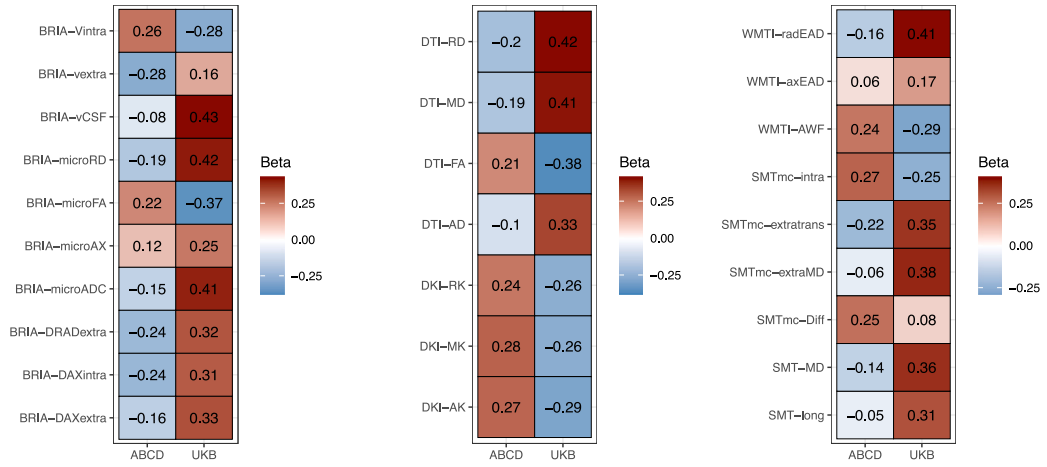

Fig. 3. Skeleton averaged scalars' age associations in ABCD and UKB data. Standardised beta coefficients are presented. BRIA = Bayesin Rotationally Invariant Approach. DKI = Diffusion Kurtosis Imaging. DTI = Diffusion Tensor Imaging. SMT = Spherical Mean Technique. SMTmc = SMT's multi-compartment version. WMTI = White Matter Tract Integrity. Metrics for each of the approaches are specified in Appendix M. Age associations in the ABCD data set were not sufficiently powered at $|r| < 0.09$. All other associations were significant ($p < 0.001$).

Table 2
Correlation of predicted and chronological age in UKB and ABCD datasets. The strongest correlations are highlighted in bold.

Model	UKB training	UKB test	ABCD training	ABCD test
BRIA	**0.6463**	**0.6476**	**0.2996**	**0.3115**
DKI	0.5463	0.5474	**0.3034**	**0.3312**
DTI	**0.6299**	**0.6272**	0.215	0.2639
SMT	0.5849	0.5834	0.2525	0.3055
SMTmc	0.5605	0.5634	0.2886	**0.3141**
WMTI	0.594	0.597	0.2071	0.2599

sex classifications (Supplement 19). Across approaches, the hippocampal cingulum presented the most consistent and strongest corrected loadings on relevant principal components, and the tract was hence examined in direct association with age. Here, 100% of the UKB age-hippocampal cingulum tract associations ($\bar{\beta}_{Training} = 0.18$, $\bar{\beta}_{Testing} = 0.19$) and 92% of the ABCD associations replicated ($\bar{\beta}_{Training} = 0.15$, $\bar{\beta}_{Testing} = 0.14$).

Just as tract-level associations, direct associations between skeleton-level scalars and age present mostly opposing trends when comparing adolescence to the mid- to late life samples (ABCD and UKB). BRIA's cerebrospinal fluid fraction, apparent diffusion coefficient, as well as both micro- and mesoscopic radial diffusivity presented the strongest age associations (Supplement O). At the same time, BRIA's intra and extra-axonal water fractions were among the largest age-associations during adolescence, together with kurtosis metrics.

3.3. White matter asymmetry

Differences between tracts present in both hemispheres show that the directionality of asymmetries are dependent on the metric and tract (Fig. 4). Most values in the left hemisphere were lower across tracts and metrics ($UKB_{training} = UKB_{validation} = 67.09\%$, $ABCD_{training} = 62.82\%$, $ABCD_{validation} = 63.68\%$), indicating rightward asymmetry or right lateralisation of tract-level diffusivity. These asymmetries were replicable within and between samples but stronger in ABCD data (absolute median Cohen's d ±mean absolute deviation: $UKB_{training} = 0.81 \pm 0.74$, $UKB_{validation} = 0.83 \pm 0.74$, $ABCD_{training} = 1.03 \pm 1.07$, $ABCD_{validation} = 1.00 \pm 1.03$).

3.4. Body mass index (BMI) and pulse pressure (PP)

As a reference, we used independent samples t-test to compare BMI and PP in the current sample ($N_{ABCD} = 4,630$, $N_{UKB} = 37,082$) to the rest of the ABCD ($N_{ABCD} = 5,410$) and UKB population ($N_{UKB} = 465,330$). The current sample presented lower PP ($d_{ABCD-Training} = -0.056$, $95\%CI[-0.095, -0.017]$, $p = 0.005$, $d_{ABCD-Test} = 0.079$, $95\%CI[-0.148, -0.011]$, $p = 0.023$, $d_{UKB-Training} = -0.033$, $95\%CI[-0.052, -0.014]$, $p = 4.382\times10^{-4}$, $d_{UKB-Testing} = -0.032$, $95\%CI[-0.061, -0.003]$, $p = 2.498 \times 10^{-4}$) and BMI ($d_{ABCD-Training} = -0.045$, $95\%CI[-0.084, -0.007]$, $p = 0.018$, $p_{ABCD-Test} = 0.171$, $d_{UKB-Training} = -0.140$, $95\%CI[-0.158, -0.123]$, $p = 2.535 \times 10^{-56}$, $d_{UKB-Testing} = -0.133$, $95\%CI[-0.159, -0.107]$, $p = 6.931 \times 10^{-26}$) compared to the rest of the respective samples.

Skeleton-level associations highlight axial kurtosis (DKI) as the strongest, replicable predictor of BMI across samples (Fig. 5). In the UKB, most metrics' were related to PP, which was replicable. This was however not the case for ABCD data.

Most principal components of white matter tract metrics could predict pulse pressure in UKB data. However, these findings did not replicate in ABCD data, and most associations between components and BMI/PP were non-significant after Bonferroni correction (Supplementary U).

3.5. Polygenic risk scores of psychiatric disorders and Alzheimer's disease

As a reference, we compared PGRS in the training samples ($N_{ABCD} = 4,117$, $N_{UKB} = 29,665$) to the rest of the ABCD dataset ($N_{ABCD} = 6,191$) and UKB population ($N_{UKB} = 377,488$), showing that PGRS were slightly lower in the present sample, but these differences were small ($d < 0.08$) and mostly non-significant for ABCD datasets (Supplementary Table Q, R).

The examined effect sizes for the PGRS associations with mean skeleton metrics were only significant in the UKB training sample for major depressive disorder, representing small effects ($|\beta| < 0.01$, Supplementary Figure S).

While the effects were small, and non-significant after Bonferroni correction, they were of the same direction and approximate strength when considered within dataset (Supplementary Figure S). Moreover, ÚKB metrics were consistently either negatively or positively associated with PGRS, independent of the disorder indicated by the score (Supplementary Figure S). Interestingly, differences in model coefficients between ABCD and UKB datasets indicated some opposing gene-brain relationships, which might be due to a lack of statistical power (Supplementary Figure S).

Similar to skeleton-average associations, when considering the first principal components of each diffusion approaches' tract scalars, only

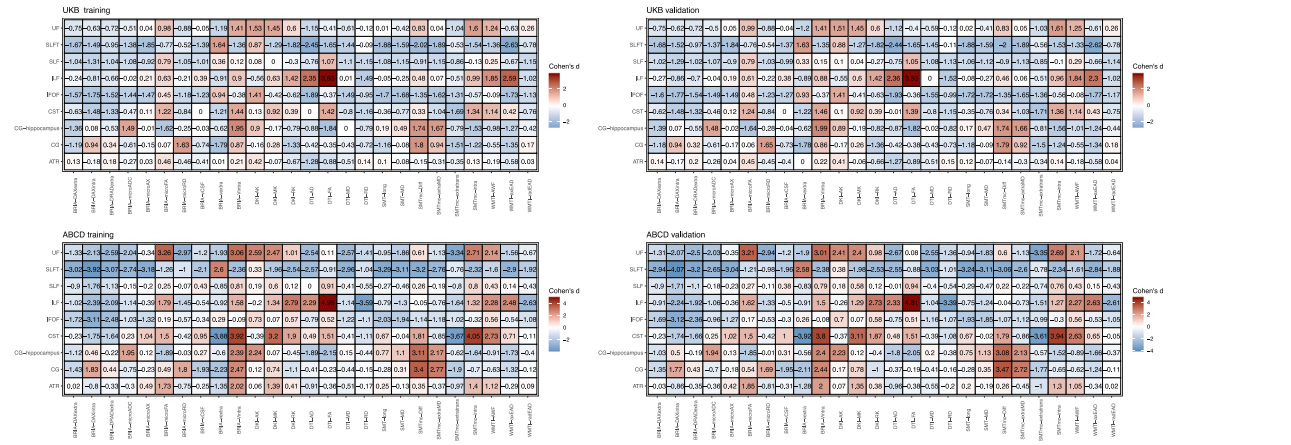

Fig. 4. Left–right tract-level differences in ABCD and UKB data. Cohen's d values are presented. BRIA = Bayesian Rotationally Invariant Approach. DKI = Diffusion Kurtosis Imaging. DTI = Diffusion Tensor Imaging. SMT = Spherical Mean Technique. SMTmc = SMT's multi-compartment version. WMTI = White Matter Tract Integrity. Metrics for each of the approaches are specified in Appendix M. UF = Uncinate Fasciculus. SLTF = Superior Longitudinal Fasciculus. SLF = Superior Longitudinal Fasciculus (temporal part). ILF = Inferior Lngitudinal Fasciculus. IFOF = Inferior Fronto-Occipial Fasciculus. CST = Cortico-Spinal Tract. CG hippocampus = Cingulum (hippocampus). CG = Cingulum (cinglate gyrus). ATR = Anterior Thalamic Radiation. Note: all $|d|_{ABCD} > 0.186$ and $|d|_{UKB} > 0.071$ were sufficiently powered. The included tracts are restricted to tracts which are present in each hemisphere separately in the John-Hopkins University tract atlas.

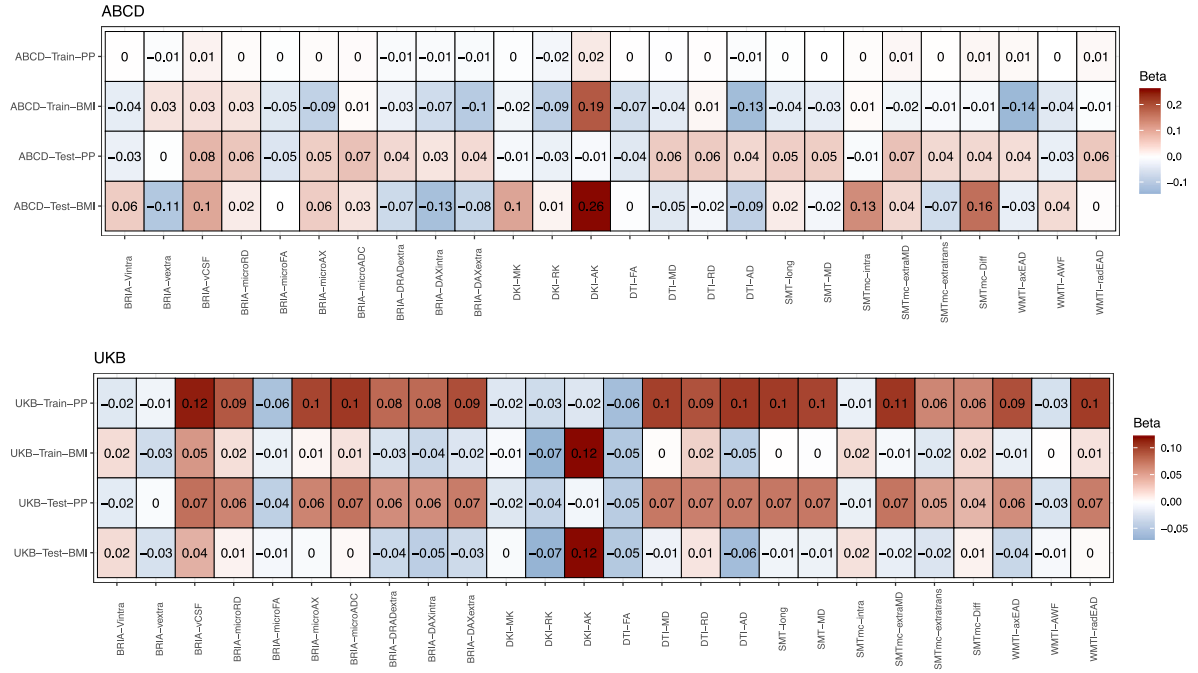

Fig. 5. Skeleton-level white matter associations with BMI and PP. Associations are indicated by standardised beta coefficients. BRIA = Bayesian Rotationally Invariant Approach. DKI = Diffusion Kurtosis Imaging. DTI = Diffusion Tensor Imaging. SMT = Spherical Mean Technique. SMTmc = SMT's multi-compartment version. WMTI = White Matter Tract Integrity. Metrics for each of the approaches are specified in Appendix M.

major depressive disorder PGRS associations were significantly associated with principal components of BRIA, DTI, and SMT in UKB (after correction for multiple testing; Supplementary Figure T). While most effects were small, and non-significant after Bonferroni correction, when considered within dataset, the effects were of the same direction and approximate strength for schizophrenia and bipolar disorder for UKB data and for OCD and bipolar disorder for ABCD data. Moreover, bipolar disorder was consistently associated with the principal component of diffusion kurtosis imaging across training and test sets. Tract metrics loading strongest on the first DKI component showed also relatively strong associations with bipolar disorder PGRS for in the superior longitudinal fasciculus ($-0.11 < \beta < -0.02$) and the inferior fronto-occipital fasciculus ($-0.08 < \beta < -0.02$).

4. Discussion

In this paper, we presented an extensive analysis of the relationship of WM parameters from multiple dMRI approaches, at the tract- and skeleton-level, and a selection of clinically relevant metrics, including sex, age, brain asymmetry, and polygenic scores for common psychiatric disorders and Alzheimer's disease. We examined one mid-life to late adulthood sample (UKB) and one adolescent sample (ABCD), with different biological characteristics. We described sample-specific sex differences in WM, WM asymmetries, and WM associations with pulse pressure, body-mass index, and polygenic risk scores. Our analyses highlight the Bayesian rotationally invariant approach principal components in approaches' components in sex classifications and age-associates. The component loadings suggested the hippocampal

cingulum tract as an important region in these associations. On the skeleton level, axial kurtosis associated strongest with BMI. Mean kurtosis and kurtosis components associated strongest with polygenic scores of bipolar disorder across datasets. However, these associations were non-significant after Bonferroni corrections. Exploratory analyses highlighted DKI component loading-based tracts of interests for bipolar disorder superior longitudinal fasciculus and inferior fronto-occipital fasciculus. Other metrics' associations, for example for PP, could not be replicated from training to test sets and across datasets, suggesting an influence of cohort characteristics, including the neurodevelopmental stage and other bio-psycho-social variables.

4.1. Sex classifications

Our analysis revealed that sex classifications based on the presented dMRI approaches are limited (Accuracy < 77%) and, for example, insufficient for clinical application. We also observed some variations in sex-prediction accuracy depending on the dataset. WMTI performed better in the ABCD dataset, BRIA in the UKB dataset, and DTI in both datasets, respectively. The variance in predictive accuracy between these datasets might be attributable to differences in participant demographics, age/neurodevelopment, or other sources of variability.

Our determination of a tract of interest was not ultimate and simply based on the selection the strongest corrected loadings of tracts on the principal components which classified sexes best, being the hippocampal cingulum tract and the uncinate fasciculus. However, standardised sex differences for these metrics were small ($\tilde{\beta} < 0.008$), reducing the practical and clinical significance of our findings on sex-differences.

Sex differences in WM microstructure reported in the literature indicate varying effects in children and adolescents (Lawrence et al., 2023; López-Vicente et al., 2021) and adults (Korbmacher et al., 2023a; Eikenes et al., 2023), and, for example, WM microstructure asymmetries were found to be similar between males and females (Korbmacher et al., 2024b). However, ageing processes reflected by microstructure parametrisation differed significantly between sexes across conventional and advanced dMRI approaches (Korbmacher et al., 2024a). The dMRI approaches which served best for sex classification in the current study (Fig. 2), contained also skeleton-level metrics showing the strongest sex differences in ageing in a previous study (Korbmacher et al., 2024a). Similar to previously obtained results using different multi-compartment approaches (Lawrence et al., 2021), we conclude that advanced dMRI models add valuable information to conventional approaches, such as DTI, when describing sex-differences.

4.2. Age associations

Principal component-based age-predictions were acceptable for UKB data ($r > 0.54$) but relatively poor for ABCD data ($r > 0.21$). One explanation for low predictive power might be found in the limited age-span in ABCD data. The principal components of the examined Bayesian approach were better predictors than other approaches' components. One potential reason is that the diffusion approach contains more metrics than all other approaches, allowing for the computation of more meaningful components.

Similarly, we examined variations in which metrics loaded on age-predicting components. That suggested that the strength of associations between WM metrics and different phenotypes might change across life, reflecting age-related changes in various phenoypes analogously. Nevertheless, across approaches, the components which explained most age variance were similar to the most important components for sex-classifications, with strongest loadings found for the hippocampal cingulum tract which presented replicable (i.e., internally and externally validated) associations ($\beta \geq 0.14$). Our findings also outline that all diffusion metrics follow individual age-associations in accordance with previous studies (Westlye et al., 2010; Korbmacher et al., 2023a, 2024a; Beck et al., 2021).

An advantage of the highlighted Bayesian approach is its capacity to dissect intra- and extra-axonal compartments may provide more sensitive insights into age-related WM degeneration associated with axonal thinning and demyelination. For example, the cerebrospinal fluid fraction and microscopic radial diffusivity presented the strongest age-associations on the skeleton level ($r = 0.44$) in UKB, suggesting an age-related loss of neuronal tissue. In contrast, the observed age-associations in ABCD showcase WM differentiation during adolescence highlighted by lower diffusivity and extra-axonal water fractions, and higher anisotropy and intra-axonal water at a higher age, as previously presented in DTI (Westlye et al., 2010). These associations largely reverse in midlife to senescence (Fig. 3). Age-related changes in WM microstructure are well-documented, and advanced dMRI adds crucial information to simpler approaches like DTI (Korbmacher et al., 2023a, 2024a; Beck et al., 2021). BRIA might be particularly useful to describe these processes due to the multiple different compartments. While the differences in diffusivity between intra- and extra-axonal space are highlighted across multi-compartment approaches, BRIA metrics might be able to provide additional information. For example, the positive age-associations of microscopic axial diffusivity in adolescence and then stronger positive association in senescence adds biologically plausible, yet additional detail to the distribution of diffusivity across compartments, likely reflecting both differentiation earlier in life and degeneration later in life (Fig. 3).

4.3. White matter asymmetry

There are a range of studies highlighting WM tract asymmetries (De Schotten et al., 2011; Arun et al., 2021). However, additional large-scale investigations are required to shed light on the mesostructural and microstructural WM asymmetry (Kong et al., 2020). One previous large-scale study in adults from mid-life to senescence demonstrated that asymmetry is present for most radiomic features, extracted from multimodal MRI, across brain regions (Korbmacher et al., 2024b). To our knowledge, there are, however, no previous large-scale investigations of WM asymmetry in both children and adolescents. Here, we provide such overview by conducting a well-powered investigation of asymmetry separately for each of these age-groups and expressed as left–right differences. Asymmetry-derived findings might reflect important neurodevelopmental steps, for instance, the lateralisation of functions, such as attention, memory, and language (Barrick et al., 2007). While we observed tract- and metric-dependent asymmetries, these asymmetries were largely replicable within and across samples. While ABCD participants presented somewhat stronger WM asymmetries ($|d| < 1.03$) across tracts than UKB ($|d| < 0.83$), the stability of tract- and metric-specific asymmetries across datasets speaks for an identification of asymmetries which are observable at different ages. Larger asymmetry in the younger ABCD sample might speak to a loss in asymmetry between childhood and older ages, as highlighted by previous studies (Mishra et al., 2013; Wahl et al., 2010; Li et al., 2012). Conversely, WM asymmetry indicated by the laterality index is positively associated with age (Korbmacher et al., 2024b), suggesting a non-linear relationship between asymmetry and age.

4.4. Cardiometabolic factors and polygenic risk score associations with WM microstructure

A growing body of evidence has presented associations between cardiometabolic factors and WM microstructure (Beck et al., 2022; Trofimova et al., 2023; Fuhrmann et al., 2019) and brain age derived from WM dMRI features (Korbmacher et al., 2023b; Beck et al., 2022). We associated body-derived parameters with multiple dMRI approaches' WM parameters using UKB and ABCD data. We revealed stronger associations of several dMRI metrics with BMI than previously presented in the ABCD dataset (Li et al., 2023), and particularly highlight skeleton-level axial kurtosis associated with BMI. Moreover,

BMI showed stronger associations with dMRI metrics in ABCD training and validation data, and with pulse pressure in UKB data, respectively. Our findings suggest that body-derived measures could be considered as a proxy for different ageing manifestations, i.e. they might have a detectable relation with WM structure and associated changes in the brain tissue.

WM associations with polygenic scores reflect previous reports of small examined effects in the UKB (Korbmacher et al., 2024a) and the ABCD datasets (Fernandez-Cabello et al., 2022). However, we find some indications of mean kurtosis associations with bipolar polygenic scores, particularly in the superior longitudinal fasciculus ($-0.11 < \beta < -0.02$) and the inferior fronto-occipital fasciculus ($-0.08 < \beta < -0.02$). These findings need however further validation, particularly in clinical samples.

Overall, the presented brain-body-gene relationships offer unique potential to establish a better understanding of developmental and ageing processes.

4.5. Limitations

Binary sex-classifications are limited to the binary sex reported in patient, registry and study reports in the UK Biobank, usually based on sex assigned at birth, potentially not considering wrong assignments/changes in sex assignments, intersex, gender, and gender-affirming treatment (including hormonal treatment), all being sources of variability. The restricted age range in the ABCD dataset and the cross-sectional study design limit the ability to interpret the findings towards ageing trends. Moreover, throughout ageing, also the clinical significance of the examined markers might change. For example, high BMI and blood pressure might be more reliable markers of cardiometabolic disorders in older adults than in adolescents. Hence, when comparing the presented WM associations one needs to keep in mind the changes of both the examined WM and associated variables, which are likely non-linear. Additionally, during maturation and ageing, interaction effects between the observed variables cannot be excluded. Additional analyses of such effects are warranted. Besides age- and other covariate dependencies in the observed associations, the associations themselves might be limited in their clinical significance. For example, the sex-classification accuracy is relatively low, either pointing to a lack of existing differences or a lack of sensitivity of the utilised white matter microstructure approaches to existing differences. Additionally, the examined samples were "more healthy" when compared to the rest of the respective cohorts indicated by significantly lower polygenic risk scores, BMI and pulse pressure.

Furthermore, the presented direct correlations of BMI and PP with white matter microstructure metrics were not corrected for crucial mediators, such as lifestyle and health behaviours, and are hence to be interpreted with caution. Lastly, the utilised acquisition protocols were similar to each other. Using different acquisition protocols, for example leveraging higher b-values, might allow to examine different effects which we were not able not observed here.

We found dMRI parameter associations with phenotypes to be highly replicable, in particular, within the same samples (comparing training and validation splits). There were, however, some restrictions on the replicability of small effects in ABCD data, including of associations between WM skeleton metrics and pulse pressure, BMI, and polygenic scores. The used ABCD sample was too small to capture effects smaller than Pearson's r=0.104 or Cohen's d=0.209 reliably. In turn, the results might contain additional bias due to a variability of the estimated diffusion metrics such as DKI (Kiselev, 2017), which might be reduced by using unified protocols/approaches (Coelho et al., 2022).

In conclusion, we analysed WM using multiple conventional and advanced dMRI approaches and related resulting parameters to metrics which are relevant to a broad range of research and clinical questions, including sex, age, brain asymmetry, BMI, PP, and polygenicity of psychiatric disorders and Alzheimer's. Our findings demonstrate that the synergy of parameters derived from advanced dMRI approaches contributes to explanations of both WM organisation and its association with the included geno- and phenotypes. This highlights the utility of multi-compartment dMRI approaches, which contain more parameters than single compartment approaches, allowing for microstructure characterisations. Moreover, the congruence in the results for the used dMRI approaches in the two datasets increases the reproducibility of the findings and adds biological detail for explaining brain maturation processes.

CRediT authorship contribution statement

Max Korbmacher: Writing – review & editing, Writing – original draft, Visualization, Validation, Software, Resources, Project administration, Methodology, Investigation, Formal analysis, Data curation, Conceptualization. **Mario Tranfa:** Writing – review & editing, Visualization, Validation. **Giuseppe Pontillo:** Writing – review & editing. **Dennis van der Meer:** Writing – review & editing, Methodology, Data curation. **Meng-Yun Wang:** Writing – review & editing. **Ole A. Andreassen:** Writing – review & editing, Resources, Funding acquisition. **Lars T. Westlye:** Writing – review & editing, Resources, Funding acquisition. **Ivan I. Maximov:** Writing – review & editing, Methodology, Funding acquisition, Data curation.

Ethical approval

This study was approved by the Norwegian Ethics Commission REK 567301, PVO 17/21624 (Ole Andreassen).

The study has been conducted using UKB data under Application 27412. UKB has received ethics approval from the National Health Service National Research Ethics Service (ref 11/NW/0382).

For the ABCD data, a centralised institutional review board approval of procedures was obtained from the University of California, San Diego. Written informed consent was obtained by a parent or guardian, and assent from the participants, before partaking in the ABCD study.

The work was performed on the Service for Sensitive Data (TSD) platform, owned by the University of Oslo, operated and developed by the TSD service group at the University of Oslo IT-Department (USIT). Computations were performed using resources provided by UNINETT Sigma2 – the National Infrastructure for High Performance Computing and Data Storage in Norway.

Funding

This research was funded by the Research Council of Norway (#223273, L.T.W.; #324252, O.A.A.); the South-Eastern Norway Regional Health Authority (#2022080, O.A.A.); and the European Union's Horizon2020 Research and Innovation Programme (#847776, O.A.A.; #802998 L.T.W.).

Declaration of competing interest

The authors declare the following competing interests: OAA has received a speaker's honorarium from Lundbeck and is a consultant to Coretechs.ai. The remaining authors declare no other competing interests.

Acknowledgements

We want to thank all UK Biobank and ABCD study facilitators and participants. Unfortunately, the most recent changes in UKB policy urge us to delete all UKB data from our servers limiting the computational reproducibility of our analyses and future research based on our dMRI data.

Supplementary material

Supplementary tables can be found in the GitHub repository https://github.com/MaxKorbmacher/dMRI_approach_comparison.

Appendix. Supplementary data

Supplementary material related to this article can be found online at https://doi.org/10.1016/j.neuroimage.2025.121132.

Data availability

Data are available from the UK Biobank https://www.ukbiobank.ac.uk and the ABCD Study https://abcdstudy.org after application. Code is available from GitHub https://github.com/MaxKorbmacher/dMRI_approach_comparison.

References

Alfaro-Almagro, Fidel, Jenkinson, Mark, Bangerter, Neal K, Andersson, Jesper LR, Griffanti, Ludovica, Douaud, Gwenaëlle, Sotiropoulos, Stamatios N, Jbabdi, Saad, Hernandez-Fernandez, Moises, Vallee, Emmanuel, et al., 2018. Image processing and quality control for the first 10,000 brain imaging datasets from UK biobank. NeuroImage 166, 400–424.

Andersson, Jesper L.R., Sotiropoulos, Stamatios N., 2016. An integrated approach to correction for off-resonance effects and subject movement in diffusion MR imaging. NeuroImage 125, 1063–1078.

Arnold, Paul D, Askland, Kathleen D, Barlassina, Cristina, Bellodi, Laura, Bienvenu, OJ, Black, Donald, Bloch, Michael, Brentani, Helena, Burton, Christie L, Camarena, Beatriz, et al., 2018. Revealing the complex genetic architecture of obsessive-compulsive disorder using meta-analysis. Mol. Psych. 23 (5), 1181–1181.

Arun, Arush Honnedevasthana, Connelly, Alan, Smith, Robert E, Calamante, Fernando, 2021. Characterisation of white matter asymmetries in the healthy human brain using diffusion MRI fixel-based analysis. Neuroimage 225, 117505.

Autism Spectrum Disorders Working Group of The Psychiatric Genomics Consortium, 2017. Meta-analysis of GWAS of over 16,000 individuals with autism spectrum disorder highlights a novel locus at 10q24. 32 and a significant overlap with schizophrenia. Mol. Autism 8, 1–17.

Barrick, Thomas R, Lawes, I Nigel, Mackay, Clare E, Clark, Chris A, 2007. White matter pathway asymmetry underlies functional lateralization. Cerebral Cortex 17 (3), 591–598.

Basser, Peter J., Mattiello, James, LeBihan, Denis, 1994. MR diffusion tensor spectroscopy and imaging. Biophys. J. 66 (1), 259–267.

Beck, Dani, de Lange, Ann-Marie G, Maximov, Ivan I, Richard, Geneviève, Andreassen, Ole A, Nordvik, Jan E, Westlye, Lars T, 2021. White matter microstructure across the adult lifespan: A mixed longitudinal and cross-sectional study using advanced diffusion models and brain-age prediction. NeuroImage 224, 117441.

Beck, Dani, de Lange, Ann-Marie G, Pedersen, Mads L, Alnæ s, Dag, Maximov, Ivan I, Voldsbekk, Irene, Richard, Geneviève, Sanders, Anne-Marthe, Ulrichsen, Kristine M, Dørum, Erlend S, et al., 2022. Cardiometabolic risk factors associated with brain age and accelerate brain ageing. HBM 43 (2), 700–720.

Camargo, Arley, 2022. PCAtest: testing the statistical significance of principal component analysis in R. PeerJ 10, e12967.

Casey, BJ, Cannonier, T, Conley, MI, Cohen, AO, Barch, DM, Heitzeg, MM, Soules, ME, Teslovich, T, Dellarco, DV, Garavan, H, Orr, CA, Wager, TD, Banich, MT, Speer, NK, Sutherland, MT, Riedel, MC, Dick, AS, Bjork, JM, Thomas, KM, Chaarani, B, Mejia, MH, Hagler, DJ Jr, Daniela Cornejo, M, Sicat, CS, Harms, MP, Dosenbach, NUF, Rosenberg, M, Earl, E, Bartsch, H, Watts, R, Polimeni, JR, Kuperman, JM, Fair, DA, Dale, AM, ABCD Imaging Acquisition Workgroup, 2018. The adolescent brain cognitive development (ABCD) study: Imaging acquisition across 21 sites. Dev. Cogn. Neurosci. 32, 43–54, http://dx.doi.org/10.1016/j.dcn.2018.03.001.

Coelho, Santiago, Baete, Steven H, Lemberskiy, Gregory, Ades-Aron, Benjamin, Barrol, Genevieve, Veraart, Jelle, Novikov, Dmitry S, Fieremans, Els, 2022. Reproducibility of the standard model of diffusion in white matter on clinical MRI systems. NeuroImage 257, 119290.

De Schotten, Michel Thiebaut, Bizzi, Alberto, Dell'Acqua, Flavio, Allin, Matthew, Walshe, Muriel, Murray, Robin, Williams, Steven C, Murphy, Declan GM, Catani, Marco, et al., 2011. Atlasing location, asymmetry and inter-subject variability of white matter tracts in the human brain with MR diffusion tractography. Neuroimage 54 (1), 49–59.

Dell'Acqua, Flavio, Tournier, J-Donald, 2019. Modelling white matter with spherical deconvolution: How and why? NMR Biomed. 32 (4), e3945.

Demontis, Ditte, Walters, Raymond K, Martin, Joanna, Mattheisen, Manuel, Als, Thomas D, Agerbo, Esben, Baldursson, Gísli, Belliveau, Rich, Bybjerg-Grauholm, Jonas, Bækvad-Hansen, Marie, et al., 2019. Discovery of the first genome-wide significant risk loci for attention deficit/hyperactivity disorder. Nat. Gen. 51 (1), 63–75.

Eikenes, Live, Visser, Eelke, Vangberg, Torgil, Håberg, Asta K, 2023. Both brain size and biological sex contribute to variation in white matter microstructure in middle-aged healthy adults. Hum. Brain Mapp. 44 (2), 691–709.

Fernandez-Cabello, Sara, Alnæ s, Dag, van der Meer, Dennis, Dahl, Andreas, Holm, Madelene, Kjelkenes, Rikka, Maximov, Ivan I, Norbom, Linn B, Pedersen, Mads L, Voldsbekk, Irene, et al., 2022. Associations between brain imaging and polygenic scores of mental health and educational attainment in children aged 9–11. NeuroImage 263, 119611.

Fieremans, Els, Jensen, Jens H., Helpern, Joseph A., 2011. White matter characterization with diffusional kurtosis imaging. Neuroimage 58 (1), 177–188.

Fuhrmann, Delia, Nesbitt, David, Shafto, Meredith, Rowe, James B, Price, Darren, Gadie, Andrew, Tyler, Lorraine K, Brayne, Carol, Bullmore, Edward T, Calder, Andrew C, et al., 2019. Strong and specific associations between cardiovascular risk factors and white matter micro-and macrostructure in healthy aging. Neurobiol. Aging 74, 46–55.

Hua, Kegang, Zhang, Jiangyang, Wakana, Setsu, Jiang, Hangyi, Li, Xin, Reich, Daniel S, Calabresi, Peter A, Pekar, James J, van Zijl, Peter CM, Mori, Susumu, 2008. Tract probability maps in stereotaxic spaces: analyses of white matter anatomy and tract-specific quantification. NeuroImage 39 (1), 336–347.

Jenkinson, Mark, Beckmann, Christian F, Behrens, Timothy EJ, Woolrich, Mark W, Smith, Stephen M, 2012. FSL. NeuroImage 62 (2), 782–790.

Jensen, Jens H, Helpern, Joseph A, Ramani, Anita, Lu, Hanzhang, Kaczynski, Kyle, 2005. Diffusional kurtosis imaging: the quantification of non-Gaussian water diffusion by means of magnetic resonance imaging. Magn. Reson. Med.: Off. J. Int. Soc. Magn. Reson. Med. 53 (6), 1432–1440.

Johnson, W. Evan, Li, Cheng, Rabinovic, Ariel, 2007. Adjusting batch effects in microarray expression data using empirical Bayes methods. Biostatistics 8 (1), 118–127.

Kaden, Enrico, Kelm, Nathaniel D, Carson, Robert P, Does, Mark D, Alexander, Daniel C, 2016a. Multi-compartment microscopic diffusion imaging. NeuroImage 139, 346–359.

Kaden, Enrico, Kruggel, Frithjof, Alexander, Daniel C., 2016b. Quantitative mapping of the per-axon diffusion coefficients in brain white matter. Magn. Reson. Med. 75 (4), 1752–1763.

Kellner, Elias, Dhital, Bibek, Kiselev, Valerij G, Reisert, Marco, 2016. Gibbs-ringing artifact removal based on local subvoxel-shifts. MR Med. 76 (5), 1574–1581.

Kiselev, Valerij G., 2017. Fundamentals of diffusion MRI physics. NMR Biomed. 30 (3), e3602.

Kong, Xiang-Zhen, Boedhoe, Premika SW, Abe, Yoshinari, Alonso, Pino, Ameis, Stephanie H, Arnold, Paul D, Assogna, Francesca, Baker, Justin T, Batistuzzo, Marcelo C, Benedetti, Francesco, et al., 2020. Mapping cortical and subcortical asymmetry in obsessive-compulsive disorder: findings from the ENIGMA consortium. Biol. Psych. 87 (12), 1022–1034.

Korbmacher, Max, de Lange, Ann Marie, van der Meer, Dennis, Beck, Dani, Eikefjord, Eli, Lundervold, Arvid, Andreassen, Ole A, Westlye, Lars T, Maximov, Ivan I, 2023a. Brain-wide associations between white matter and age highlight the role of fornix microstructure in brain ageing. HBM 44 (10).

Korbmacher, Max, Gurholt, Tiril P, de Lange, Ann-Marie G, van der Meer, Dennis, Beck, Dani, Eikefjord, Eli, Lundervold, Arvid, Andreassen, Ole A, Westlye, Lars T, Maximov, Ivan I, 2023b. Bio-psycho-social factors' associations with brain age: a large-scale UK biobank diffusion study of 35,749 participants. Front. Psych. 14, 1117732.

Korbmacher, Max, van der Meer, Dennis, Beck, Dani, Askeland-Gjerde, Daniel E, Eikefjord, Eli, Lundervold, Arvid, Andreassen, Ole A, Westlye, Lars T, Maximov, Ivan I, 2024a. Distinct longitudinal brain white matter microstructure changes and associated polygenic risk of common psychiatric disorders and alzheimer's disease in the UK biobank. Biol. Psychiatry Glob. Open Sci. 100323.

Korbmacher, Max, van der Meer, Dennis, Beck, Dani, de Lange, Ann-Marie G, Eikefjord, Eli, Lundervold, Arvid, Andreassen, Ole A, Westlye, Lars T, Maximov, Ivan I, 2024b. Brain asymmetries from mid-to late life and hemispheric brain age. Nat. Commun. 15 (1), 956.

Lawrence, Katherine E, Abaryan, Zvart, Laltoo, Emily, Hernandez, Leanna M, Gandal, Michael J, McCracken, James T, Thompson, Paul M, 2023. White matter microstructure shows sex differences in late childhood: Evidence from 6797 children. Hum. Brain Mapp. 44 (2), 535–548.

Lawrence, Katherine E, Nabulsi, Leila, Santhalingam, Vigneshwaran, Abaryan, Zvart, Villalon-Reina, Julio E, Nir, Talia M, Ba Gari, Iyad, Zhu, Alyssa H, Haddad, Elizabeth, Muir, Alexandra M, et al., 2021. Age and sex effects on advanced white matter microstructure measures in 15,628 older adults: A UK biobank study. Brain Imaging Behav. 15 (6), 2813–2823.

Li, Zhaolong Adrian, Cai, Yuqi, Taylor, Rita L, Eisenstein, Sarah A, Barch, Deanna M, Marek, Scott, Hershey, Tamara, 2023. Associations between socioeconomic status, obesity, cognition, and white matter microstructure in children. JAMA Netw. Open 6 (6), e2320276–e2320276.

Li, Yi-Ou, Yang, Fanpei G, Nguyen, Christopher T, Cooper, Shelly R, LaHue, Sara C, Venugopal, Sandya, Mukherjee, Pratik, 2012. Independent component analysis of DTI reveals multivariate microstructural correlations of white matter in the human brain. Hum. Brain Mapp. 33 (6), 1431–1451.

López-Vicente, Mónica, Lamballais, Sander, Louwen, Suzanne, Hillegers, Manon, Tiemeier, Henning, Muetzel, Ryan L, White, Tonya, 2021. White matter microstructure correlates of age, sex, handedness and motor ability in a population-based sample of 3031 school-age children. Neuroimage 227, 117643.

Maximov, Ivan I., Alnæs, Dag, Westlye, Lars T., 2019. Towards an optimised processing pipeline for diffusion magnetic resonance imaging data: Effects of artefact corrections on diffusion metrics and their age associations in UK biobank. Hum. Brain Mapp. 40 (14), 4146–4162.

Maximov, Ivan I, van Der Meer, Dennis, de Lange, Ann-Marie G, Kaufmann, Tobias, Shadrin, Alexey, Frei, Oleksandr, Wolfers, Thomas, Westlye, Lars T, 2021. Fast quality control method for derived diffusion metrics (YTTRIUM) in big data analysis: UK biobank 18,608 example. HBM 42 (10), 3141–3155.

Miller, Karla L, Alfaro-Almagro, Fidel, Bangerter, Neal K, Thomas, David L, Yacoub, Essa, Xu, Junqian, Bartsch, Andreas J, Jbabdi, Saad, Sotiropoulos, Stamatios N, Andersson, Jesper LR, et al., 2016. Multimodal population brain imaging in the UK biobank prospective epidemiological study. Nat. Neur. 19 (11), 1523–1536.

Mishra, Virendra, Cheng, Hua, Gong, Gaolang, He, Yong, Dong, Qi, Huang, Hao, 2013. Differences of inter-tract correlations between neonates and children around puberty: a study based on microstructural measurements with DTI. Front. Hum. Neurosci. 7, 721.

Mori, S., Wakana, S., Nagae-Poetscher, L.M., Van Zijl, PCM, 2006. MRI atlas of human white matter. Am. J. Neurorad. 27 (6), 1384.

Mullins, Niamh, Forstner, Andreas J, O'Connell, Kevin S, Coombes, Brandon, Coleman, Jonathan RI, Qiao, Zhen, Als, Thomas D, Bigdeli, Tim B, Børte, Sigrid, Bryois, Julien, et al., 2021. Genome-wide association study of more than 40,000 bipolar disorder cases provides new insights into the underlying biology. Nat. Gen. 53 (6), 817–829.

Novikov, Dmitry S, Fieremans, Els, Jespersen, Sune N, Kiselev, Valerij G, 2019. Quantifying brain microstructure with diffusion MRI: Theory and parameter estimation. NMR Biomed. 32 (4), e3998.

Novikov, Dmitry S., Kiselev, Valerij G., Jespersen, Sune N., 2018a. On modeling. Magn. Reson. Med. 79 (6), 3172–3193.

Novikov, Dmitry S, Veraart, Jelle, Jelescu, Ileana O, Fieremans, Els, 2018b. Rotationally-invariant mapping of scalar and orientational metrics of neuronal microstructure with diffusion MRI. NeuroImage 174, 518–538.

Nygaard, Vegard, Rødland, Einar Andreas, Hovig, Eivind, 2016. Methods that remove batch effects while retaining group differences may lead to exaggerated confidence in downstream analyses. Biostatistics 17 (1), 29–39.

Otowa, Takeshi, Hek, Karin, Lee, Minyoung, Byrne, Enda M, Mirza, Saira S, Nivard, Michel G, Bigdeli, Timothy, Aggen, Steven H, Adkins, Daniel, Wolen, Aaron, et al., 2016. Meta-analysis of genome-wide association studies of anxiety disorders. Mol. Psych. 21 (10), 1391–1399.

Privé, Florian, Arbel, Julyan, Vilhjálmsson, Bjarni J., 2020. LDpred2: better, faster, stronger. Bioinformatics 36 (22–23), 5424–5431.

Reisert, Marco, Kellner, Elias, Dhital, Bibek, Hennig, Juergen, Kiselev, Valerij G, 2017. Disentangling micro from mesostructure by diffusion MRI: a Bayesian approach. Neuroimage 147, 964–975.

Smith, Stephen M., 2002. Fast robust automated brain extraction. HBM 17 (3), 143–155.

Smith, Stephen M, Jenkinson, Mark, Johansen-Berg, Heidi, Rueckert, Daniel, Nichols, Thomas E, Mackay, Clare E, Watkins, Kate E, Ciccarelli, Olga, Cader, M Zaheer, Matthews, Paul M, et al., 2006. Tract-based spatial statistics: voxelwise analysis of multi-subject diffusion data. NeuroImage 31 (4), 1487–1505.

Smith, Stephen M, Jenkinson, Mark, Woolrich, Mark W, Beckmann, Christian F, Behrens, Timothy EJ, Johansen-Berg, Heidi, Bannister, Peter R, De Luca, Marilena, Drobnjak, Ivana, Flitney, David E, et al., 2004. Advances in functional and structural MR image analysis and implementation as FSL. NeuroImage 23, S208–S219.

Sudlow, Cathie, Gallacher, John, Allen, Naomi, Beral, Valerie, Burton, Paul, Danesh, John, Downey, Paul, Elliott, Paul, Green, Jane, Landray, Martin, et al., 2015. UK biobank: an open access resource for identifying the causes of a wide range of complex diseases of middle and old age. PLoS Med. 12 (3), e1001779.

Trofimova, Olga, Latypova, Adeliya, DiDomenicantonio, Giulia, Lutti, Antoine, de Lange, Ann-Marie G, Kliegel, Matthias, Stringhini, Silvia, Marques-Vidal, Pedro, Vaucher, Julien, Vollenweider, Peter, et al., 2023. Topography of associations between cardiovascular risk factors and myelin loss in the ageing human brain. Commun. Biol. 6 (1), 392.

Trubetskoy, Vassily, Pardiñas, Antonio F, Qi, Ting, Panagiotaropoulou, Georgia, Awasthi, Swapnil, Bigdeli, Tim B, Bryois, Julien, Chen, Chia-Yen, Dennison, Charlotte A, Hall, Lynsey S, et al., 2022. Mapping genomic loci implicates genes and synaptic biology in schizophrenia. Nat 604 (7906), 502–508.

Veraart, Jelle, Fieremans, Els, Novikov, Dmitry S., 2016. Diffusion MRI noise mapping using random matrix theory. MR Med. 76 (5), 1582–1593.

Wahl, Michael, Li, Yi-Ou, Ng, Joshua, LaHue, Sara C, Cooper, Shelly R, Sherr, Elliott H, Mukherjee, Pratik, 2010. Microstructural correlations of white matter tracts in the human brain. Neuroimage 51 (2), 531–541.

Westlye, Lars T, Walhovd, Kristine B, Dale, Anders M, Bjørnerud, Atle, Due-Tønnessen, Paulina, Engvig, Andreas, Grydeland, Håkon, Tamnes, Christian K, Østby, Ylva, Fjell, Anders M, 2010. Life-span changes of the human brain white matter: diffusion tensor imaging (DTI) and volumetry. Cerebral Cortex 20 (9), 2055–2068.

Wightman, Douglas P, Jansen, Iris E, Savage, Jeanne E, Shadrin, Alexey A, Bahrami, Shahram, Holland, Dominic, Rongve, Arvid, Børte, Sigrid, Winsvold, Bendik S, Drange, Ole Kristian, et al., 2021. A genome-wide association study with 1,126,563 individuals identifies new risk loci for Alzheimer's disease. Nat. Gen. 53 (9), 1276–1282.

Wray, Naomi R, Ripke, Stephan, Mattheisen, Manuel, Trzaskowski, Maciej, Byrne, Enda M, Abdellaoui, Abdel, Adams, Mark J, Agerbo, Esben, Air, Tracy M, Andlauer, Till MF, et al., 2018. Genome-wide association analyses identify 44 risk variants and refine the genetic architecture of major depression. Nat. Gen. 50 (5), 668–681.